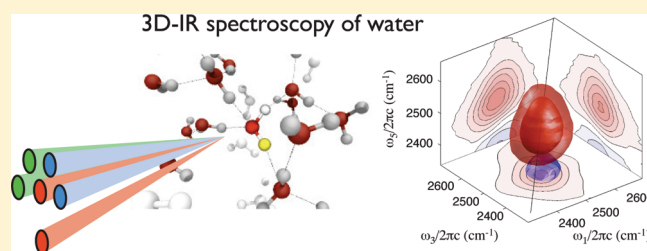


# Three-Dimensional Infrared Spectroscopy of Isotope-Substituted Liquid Water Reveals Heterogeneous Dynamics

Sean Garrett-Roe,<sup>†</sup> Fivos Perakis,<sup>†</sup> Francesco Rao,<sup>‡</sup> and Peter Hamm<sup>\*,†</sup><sup>†</sup>Institute of Physical Chemistry, University of Zurich, Zurich, Switzerland<sup>‡</sup>Freiburg Institute for Advanced Studies (FRIAS), University of Freiburg, Freiburg, Germany Supporting Information

**ABSTRACT:** The dynamics of the hydrogen bond network of isotopically substituted liquid water are investigated with a new ultrafast nonlinear vibrational spectroscopy, three-dimensional infrared spectroscopy (3D-IR). The 3D-IR spectroscopy is sensitive to three-point frequency fluctuation correlation functions, and the measurements reveal heterogeneous structural relaxation dynamics. We interpret these results as subensembles of water which do not interconvert on a half picosecond time scale. We connect the experimental results to molecular dynamics (MD) simulations, performing a line shape analysis as well as complex network analysis.



## INTRODUCTION

Since Röntgen,<sup>1</sup> researchers have speculated about inhomogeneous structures in ambient liquid water. It is well-understood that, as a liquid is supercooled, it develops both structural and dynamical heterogeneities,<sup>2,3</sup> which occur when the fluid is no longer uniform; for example, jamming occurs, and different domains develop different structures. In ambient water, small-angle X-ray scattering experiments<sup>4</sup> have recently been interpreted as evidence of structural heterogeneities on the 1 nm length-scale, though not without controversy.<sup>5–7</sup> Liquid water is a highly dynamic medium, of course, and its hydrogen bond network reorganizes on a picosecond time scale.<sup>8–18</sup> Here we apply a new multidimensional ultrafast infrared technique, three-dimensional infrared spectroscopy (3D-IR), to isotopically substituted liquid water at ambient conditions. We observe that the structural relaxation dynamics are heterogeneous and that water contains a mixture of distinct subensembles which do not intermix on a half picosecond time scale.

Whether liquid water should be considered one uniform, homogeneous fluid or a mixture of two or more distinct sub-species is a long-standing, unresolved, and controversial question. Many researchers have tried to identify spectroscopically distinct subensembles of hydrogen bonding using multiple pulse IR spectroscopies.<sup>8–11,14,15,18,19</sup> Experiments using IR and Raman spectroscopy, for example, have examined wavelength-dependent rates of orientational relaxation,<sup>8,19</sup> vibrational relaxation,<sup>10,15,19,20</sup> and spectral diffusion.<sup>21</sup> The evidence in the literature weighs on both sides of the argument. Perhaps foremost, the presence of an isosbestic point in the OH-stretching band of water as a function of temperature<sup>19,22</sup> has long been seen as the proverbial smoking gun of two-state behavior. A simple thermodynamic analysis, however, shows that this is not necessarily so;<sup>20,23</sup> isosbestic

points can appear in a completely homogeneous system. The pathways of vibrational relaxation suggest vibrational subbands associated with strongly and weakly hydrogen bonded waters which are distinct on a 2–10 ps time scale.<sup>15</sup> On the other hand, the analysis of 2D-IR lineshapes and molecular dynamics (MD) simulations say that these hydrogen bonds are broken only fleetingly ( $\sim 200$  fs), much as a transition state or saddle point is only transiently populated.<sup>24</sup> Similar fundamental disagreements occur in the context of water around ions<sup>25–27</sup> and water around hydrophobes.<sup>28–30</sup>

It is meaningful to consider a fluid heterogeneous if it has multiple, distinct rates of structural relaxation. Here we demonstrate that 3D-IR spectroscopy can report whether or not structural relaxation rates in liquid water remain distinct through a three-point frequency fluctuation correlation function. The measurements show heterogeneity which persists on a half picosecond time scale. The results are interpreted using a complex network analysis of MD simulations of water which provides a molecular description of the multiple local free-energy minima generating the heterogeneous dynamics.

**Theoretical Foundations.** Ultrafast vibrational spectroscopy is useful to probe structural dynamics in liquid water because water's vibrational frequencies depend on the local structure.<sup>10,14,18,31,32</sup> The most common vibrational marker modes are the stretching vibrations of isotope diluted water; in this work, we use the OD vibration of HOD in H<sub>2</sub>O. For example, 2D-IR spectroscopy<sup>12,13,16</sup> measures diffusion of the OD vibrator in frequency space (spectral diffusion), which is directly connected

Received: March 1, 2011

Revised: April 27, 2011

Published: May 11, 2011

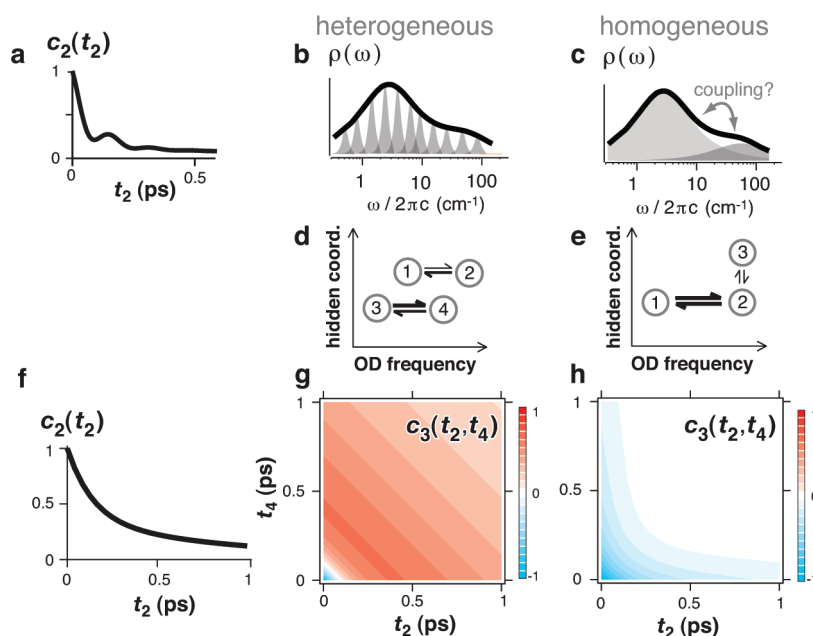


**Figure 1.** 3D-IR distinguishing heterogeneous and homogeneous broadening of low-frequency (intermolecular) modes. (a) The two-point frequency fluctuation correlation function,  $c_2(t_2)$ , of water<sup>14</sup> as deduced from 2D-IR spectroscopy. (b–c) The Fourier transform of  $c_2(t_2)$  is the spectral density,  $\rho(\omega)$ . This is essentially a one-dimensional spectrum of the low-frequency modes to which the OD-stretch oscillator is coupled. This spectral density cannot distinguish whether structural relaxation is heterogeneous (b) or homogeneous (c) or detect coupling between modes. (d–e) Models demonstrating heterogeneous and homogeneous relaxation dynamics. OD-stretch frequency fluctuations are represented by transitions between states governed by rate equations. Heterogeneous dynamics are the sum of uncorrelated processes (d), while homogeneous dynamics involve a hidden coordinate coupled to the OD-stretch frequency (e). (f) The models (d–e) generate equivalent two-point correlation functions  $c_2$ . (g–h) The three-point correlation functions,  $c_3$ , are distinguishable. Heterogeneous dynamics depend only on the total population time,  $t_2 + t_4$ , so lines of constant value run at a 45° angle (g), while homogeneous dynamics cause curved contour lines (h).

to diffusion of a water molecule in real space. Conceptually speaking, the 2D-IR pulse sequence interrogates the OD vibrator by first tagging an initial OD vibrational frequency; then the environment around the OD evolves during a time  $t_2$ ; finally, the sequence reads out the resulting vibrational frequency.

By changing  $t_2$ , 2D-IR can measure how quickly the system loses memory of the initial excitation frequency, mapping out an ensemble average two-point frequency fluctuation correlation function

$$c_2(t_2) = \langle \delta\omega(t_2) \delta\omega(0) \rangle \quad (1)$$

where  $\delta\omega(t)$  is the instantaneous deviation of the frequency from the mean  $\delta\omega(t) = \omega(t) - \langle \omega \rangle$ . Experiments<sup>12,13,16</sup> and theory<sup>11,14,18,32–34</sup> have shown the loss of correlation due to specific motions of water molecules: librational motions on a  $\sim 50$  fs time scale, intermolecular O–O vibrations on a 150 fs time scale, and collective reorganization of the fluid on a  $\sim 1$  ps time scale (Figure 1a).

Descriptors like eq 1 do not report whether dynamics are heterogeneous or not. Inside the ensemble average of eq 1, every OD bond has a different frequency trajectory, but that of course does not mean the dynamics is heterogeneous. A statistically meaningful way to characterize the dynamic heterogeneity is to define a two-point correlation function for subensembles. Specifically, if molecule  $i$  has frequency fluctuations  $\delta\omega_i(t)$ , then its two-point correlation function for over a finite time window  $T$  can be written

$$c_2^{(i)}(t; T) = \frac{1}{T} \int_0^T d\tau \delta\omega_i(\tau + t) \delta\omega_i(\tau) \quad (2)$$

If the system is ergodic, then as  $T$  approaches infinity the  $c_2^{(i)}(t; T \rightarrow \infty)$  must equal the ensemble average  $c_2(t)$ . If over some finite time  $T$ ,  $c_2^{(i)}(t; T)$  is different for different individual molecules  $i$ , or different subensembles of molecules, then one can say the dynamics is heterogeneous on time scale  $T$ . For glasses, this is certainly the case.<sup>3</sup> Whether or not this is the case for water is an open question we aim to address.

The essential difficulties faced by spectroscopies like 2D-IR to establish or refute the existence subensembles in liquid water are 3-fold. First, these subensembles are not distinctly resolved with respect to the OD stretch frequency. Second, if the time scales are similar (within a factor  $\approx 3$ ), it is essentially impossible to distinguish a mono- from a multiexponential decay. Third, even if a biexponential decay of whatever spectroscopic quantity can be identified, this is not yet a sufficient piece of evidence to assign the relaxation to a heterogeneous mechanism. As Berg et al.<sup>35</sup> have demonstrated in the optical regime, heterogeneous and homogeneous relaxation mechanisms can generate identical decays. The same conclusion was reached in the context of solvation dynamics in nonequilibrium 2D-IR spectroscopy; fast and slow solvation modes can be coupled, or not, and third-order spectroscopy cannot resolve this.<sup>36</sup>

To understand the limitations of 2D-IR spectroscopy, consider the  $c_2$  derived from a 2D-IR measurement (Figure 1a). The Fourier transform of  $c_2$  is a one-dimensional spectral density, that is, a spectrum of the low-frequency intermolecular modes ( $\lesssim 300$  cm<sup>−1</sup>) to which the OD-stretch is coupled (Figure 1b–c). The line broadening mechanism of these low-frequency modes contains nontrivial information about the structural relaxation of the fluid.<sup>37</sup> At one extreme, if the

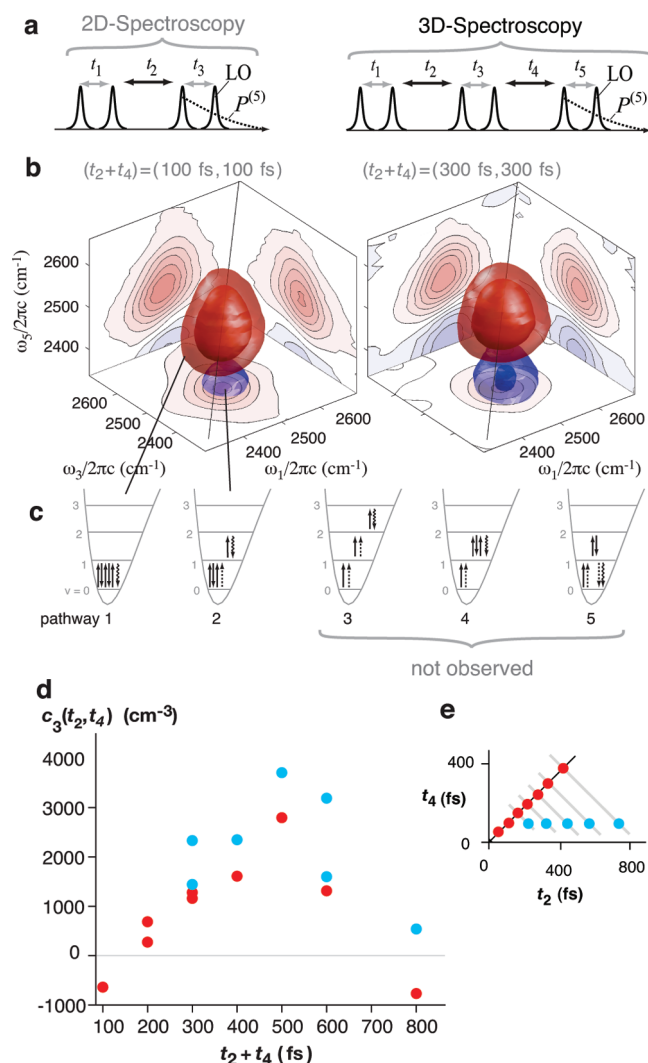


**Figure 2.** 3D-IR spectra of the OD-stretch. (a) Comparison of 3D-IR and 2D-IR pulse sequences. (b) 3D-IR spectra for population times  $(t_2, t_4) = (100 \text{ fs}, 100 \text{ fs})$  and  $(300 \text{ fs}, 300 \text{ fs})$ . (c) Wave mixing diagrams of the five possible pathways up and down the vibrational ladder which can in principle be observed in a 3D-IR experiment. (d) The three-point correlation function extracted from the 3D-IR spectra,  $c_3(t_2, t_4)$  indicates heterogeneous relaxation dynamics. (e) The time scheme for the  $c_3(t_2, t_4)$  data parallel to the  $t_2$ -axis (with  $t_4 = 100 \text{ fs}$ , blue) and  $(t_2, t_4)$ -diagonal (red).

low-frequency modes of a system are homogeneously broadened (Figure 1c), then all vibrational chromophores will have the same rates of structural relaxation, that is, eq 2 gives the same result for all molecules. The structural relaxation dynamics are homogeneous despite the fact that different waters are not identical at any given instant of time as they sample the many hydrogen bonding conformations available in the liquid. At the other extreme, if the low-frequency modes are inhomogeneously broadened (Figure 1b), then water molecules in different environments will have different structural relaxation rates; in that sense, the relaxation dynamics are heterogeneous, and different molecules would generate different relaxation rates in eq 2. Real systems will lie between these two extremes, and the term “heterogeneous” is, of course, a matter of time scale (the  $T$  in eq 2). Nevertheless, just as linear spectroscopy cannot distinguish line broadening mechanisms in the high-frequency OD-stretch, 2D-IR spectroscopy

cannot distinguish line broadening mechanisms of the low-frequency intermolecular modes to which the OD-stretch is coupled. Homogeneous and heterogeneous structural relaxation dynamics may give rise to identical spectral densities (Figure 1b–c).

Equation 2 is an intuitive description of heterogeneous dynamics (different subensembles have different dynamics), but this metric of heterogeneity cannot be extracted from standard IR spectra of water because of the extensive overlap along the frequency axis.<sup>38</sup> If there were more structure in the vibrational spectrum—two distinct features, for example—then there would be a clear way to define two initial subensembles, and the connection to eq 2 would be straightforward. No such separation in water exists, however, so one cannot extract the information embodied in eq 2 from 2D-IR spectra and ultimately cannot definitively assign homogeneous or heterogeneous dynamics.

Fifth-order spectroscopies like 3D-IR<sup>37,39</sup> and related techniques<sup>35,36,40</sup> can distinguish these structural relaxation mechanisms. In a 3D-IR pulse sequence, the OD frequency is labeled by three pairs of pulses as a function of two waiting times ( $t_2$  and  $t_4$ ) (Figure 2a). This makes 3D-IR closely related to a three-point correlation function,<sup>41</sup>

$$c_3(t_2, t_4) = \langle \delta\omega(t_2 + t_4) \delta\omega(t_2) \delta\omega(0) \rangle \quad (3)$$

which is nonzero because the OD absorption line is asymmetric, and the dynamics is non-Gaussian. These third-order correlations are a 2D function of the two time coordinates,  $t_2$  and  $t_4$ . The extra information encoded by this additional degree of freedom makes 3D-IR able to distinguish heterogeneous (Figure 1g) from homogeneous (Figure 1h) relaxation dynamics. If we were to make a 2D Fourier transform of the three-point correlation function  $c_3(t_2, t_4)$ , it would then be a 2D spectrum of the low-frequency modes. Expressed in either the time- or the frequency-domain, precisely this information content motivates research toward 2D-Raman<sup>42–45</sup> or 2D-THz experiments,<sup>45</sup> neither of which is yet experimentally feasible for water. Higher-order pulse sequences, which are sensitive to higher-order time correlation functions, have also been used for the same purpose in theoretical studies<sup>46</sup> and in NMR experiments<sup>47</sup> on polymers near the glass transition.

Experimentally, it is not yet feasible to measure the full two-dimensional three-point correlation function pictured in Figure 1g–h. Nevertheless, a reduced measurement still carries the essential information, as illustrated by the following models of dynamics in frequency space. These models represent the dynamics in frequency space as discrete states coupled by chemical kinetics. In Figure 1d, fast and slow frequency fluctuations are uncoupled, so the dynamics are heterogeneous; in Figure 1e the fast and slow processes are coupled, so the dynamics are homogeneous. The two systems depicted have mathematically identical, nonexponential two-point correlation functions (Figure 1f), but clearly distinguishable three-point correlation functions. Any system which has a single exponential response will have higher order correlation functions that are only a function of the sum of times, because  $e^{-t}e^{-t'} = e^{-(t+t')}$ . An uncorrelated sum of such processes, that is, heterogeneous dynamics (Figure 1d), naturally has this same property even though the ensemble averaged  $c_2(t_2)$  is nonexponential. As a result,  $c_3(t_2, t_4)$  depends only on the total population time,  $t_2 + t_4$  (Figure 1g), and the contour lines run at  $-45^\circ$ . On the other hand, any inherently multiexponential process, that is, homogeneous dynamics (Figure 1e), in which the different processes



are coupled, will not have the property, and values of  $c_3$  along pathways with the same total time  $t_2 + t_4$  will differ; this difference is the biggest between pathways on the axis and diagonal (Figure 1h). This feature of the three-point correlation function is what the experiment is designed to capture, allowing us to assign the observed dynamics to a heterogeneous or a homogeneous structural relaxation.

## MATERIAL AND METHODS

**Data Acquisition.** A 1 kHz titanium sapphire amplifier pumped a home-built OPA, generating 2  $\mu$ J pulses centered at 2500  $\text{cm}^{-1}$  with enough bandwidth (300  $\text{cm}^{-1}$ ) to cover the  $\nu = 0-1$  of the OD-stretch (170  $\text{cm}^{-1}$ ). Pulses were precompressed using optical materials of opposite dispersion to null the second-order dispersion due to materials in the interferometer.<sup>48</sup> The emitted signal field  $E_s$  was overlapped with the local oscillator  $E_{LO}$  on opposite sides of a 50% beam splitter for balanced detection.<sup>49</sup> The signal from pairs of pixels of the MCT array detector (2 rows of 32 pixels, Infrared Assoc.) were differenced prior to integration, amplification, and digitization. To remove unwanted scattering signals, we phase cycled the last interaction  $E_5$  at 500 Hz using a photoelastic modulator (PEM) (Hinds Instruments).<sup>50</sup> The interferograms were scanned in steps of 23 fs (undersampling 3) and subsequently zero-padded and Fourier transformed for a final resolution of 35  $\text{cm}^{-1}$  along  $\omega_1$  and  $\omega_3$ .<sup>51</sup> The spectrometer resolution for  $\omega_5$  was  $\sim 10 \text{ cm}^{-1}$ .

The sample was 5% HOD/ $\text{H}_2\text{O}$  film of 6  $\mu\text{m}$  thickness held between two  $\text{CaF}_2$  windows at room temperature. In the sample cell was a 2.5  $\mu\text{m}$  thick Ni-alloy pinhole of 5  $\mu\text{m}$  diameter (custom Thorlabs) used for phasing spectra.<sup>39,52</sup>

**Molecular Dynamics Simulations.** For the MD simulations, we use the Gromacs package<sup>53</sup> in the NVT ensemble, with 1019 SPC-water molecules at 300 K at experimental density and 2 fs time steps. The instantaneous frequency shift of the OD vibration is treated with second-order perturbation theory,<sup>54</sup> resulting in a linear dependence of the frequency on the mass-weighted forces from the surrounding waters projected on the OD bond, similar to ref 55. The frequency trajectory is integrated according to eq 6 of ref 41 on a  $48 \times 48 \times 48$  grid with an effective 40 fs time spacing, and purely absorptive 3D spectra are calculated.<sup>39,41</sup> The simulated spectra are then analyzed according to eq 4, just as the experimental data are. The extracted  $c_3$  is insensitive to the grid extent and grid spacing when the windowing function is used as with the experimental data. For details of the complex network analysis, see ref 56.

## RESULTS

**Experimental Section.** Figure 2b shows purely absorptive 3D-IR spectra of the OD-vibration of 5% HOD in  $\text{H}_2\text{O}$  at room temperature for different sets of waiting times ( $t_2, t_4$ ). The laser and interferometer to generate the 3D pulse sequence were described previously,<sup>39</sup> except that for these experiments the pulses were 300  $\text{cm}^{-1}$  broad, full-width-at-half-maximum, and the pulses are compressed to null second-order dispersion (Materials and Methods). The 3D-IR spectra have complicated three-dimensional shapes which change with the population times,  $t_2$  and  $t_4$  (Supporting Information, Movies 1 and 2). The intensity of the 3D-IR spectrum scales linearly with the concentration of HOD, which verifies that this is a direct fifth-order signal and not a cascaded third-order signal.<sup>39,57</sup>

(Appendix). Each 3D-IR spectrum has two lobes: the first, in red, corresponds to all interactions taking place between the  $\nu = 0$  and  $\nu = 1$  vibrational levels; the second, in blue, is in a vibrational coherence between the  $\nu = 1$  and  $\nu = 2$  levels during  $t_5$ . In general, there are five possible pathways up and down the vibrational ladder in a 3D-IR experiment (Figure 2c); these were clearly observed for the asymmetric stretch of  $\text{CO}_2$  in  $\text{H}_2\text{O}$ .<sup>39</sup> It is not surprising that the highest lying transition, accessing the third excited state, is not observed here, because it is outside of the laser bandwidth. Two other pathways that might be expected on the grounds of bandwidth alone, however, are not observed. We interpret the strong suppression of these bands to be due to the combination of the laser bandwidth and faster dephasing dynamics during the  $|1\rangle\langle 2|$  coherence (Appendix).

From the 0–1 band of 3D-IR spectra (pathway 1, Figure 2C), the three-point correlation function,  $c_3$ , can be extracted by calculating a weighted average over the band

$$c_3(t_2, t_4) = \iiint d(\delta\omega_1) d(\delta\omega_3) d(\delta\omega_5) \delta\omega_1 \delta\omega_3 \delta\omega_5 \times R_1^{(s)}(\delta\omega_1, t_2, \delta\omega_3, t_4, \delta\omega_5) B^{(s)}(\delta\omega_1, \delta\omega_3, \delta\omega_5) \quad (4)$$

where  $R_1^{(s)}$  is the 0–1 band of the 3D-IR spectrum and  $B^{(s)}$  is a 150  $\text{cm}^{-1}$  full-width at half-maximum Gaussian window function to suppress the effect of noise at the edges of the spectrum (Appendix). This method is an approximation of the true underlying correlation function due to the effects of motional narrowing, overlapping bands, and the non-Condon effect. Note that, just as in 2D-IR,<sup>24</sup> the inertial response of the librations, which are the fastest motions in the liquid, are suppressed in the extracted correlation function due to motional narrowing. All motions slower than the librations remain well-resolved, allowing us to measure the relaxation processes associated with reorganizing the hydrogen-bond network.

We determined  $c_3$  from spectra measured parallel to the  $t_2$ -axis, (with  $t_4 = 100$  fs to avoid artifacts due to pulse overlap, Figure 2d–e, blue), and along the diagonal of the  $(t_2, t_4)$ -space (Figure 2d–e, red). The  $c_3$  quantitatively characterizes the spectra's complicated 3D shapes. The  $c_3$  is a dynamical skewness because it is the third central moment of a dynamic distribution (eq 3). The value of  $c_3$  increases and then decreases (Figure 2d), indicating at least two relaxation processes with similar rates and opposite skewness. Initially the spectrum is skewed slightly to low frequencies, causing  $c_3$  to be slightly negative. In the first few hundred femtoseconds, the structural dynamics destroy the correlations on the red side of the spectrum faster than on the blue side of the spectrum. The 3D spectrum then appears skewed to high frequency, leading to a positive value of  $c_3$ . The  $c_3$  finally decays to zero, within signal-to-noise, by 800 fs.

Strikingly, the values of  $c_3(t_2, t_4)$  are nearly identical parallel to the  $t_2$ -axis and along the diagonal, so are a function of the total time  $t_2 + t_4$  only. This is a strong indication of heterogeneous dynamics on these time scales. We consider this the most important result of the paper.

**Lineshape Analysis.** The  $c_3$  can also be calculated from MD simulations. The method we have used (Materials and Methods) makes a number of approximations, namely, the Condon approximation (i.e., the oscillator strength is constant) and an empirical mapping from forces to frequency. Nevertheless, it has proved very successful at explaining correlation functions extracted from 2D-IR spectra.<sup>12,14,16,32,58</sup> We show the exact three-point frequency fluctuation correlation function calculated with a

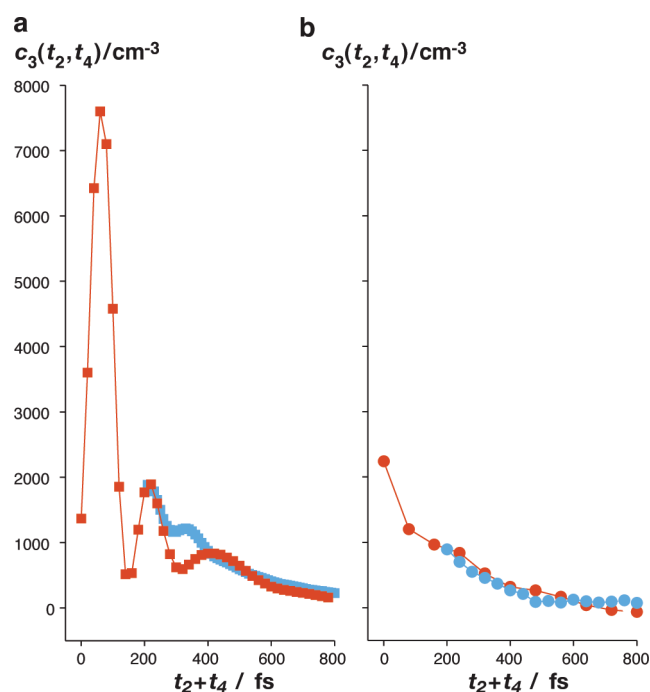


**Figure 3.** Lineshape analysis from MD simulations. (a) The  $c_3$  calculated directly from a frequency trajectory using the same weighting function  $B^{(5)}$  as in eq 4 along the same paths in  $(t_2, t_4)$  as the experiment (Figure 2d,e), and (b) similarly, extracted from simulated 3D-IR spectra.

histogram-based method<sup>38</sup> (Figure 3a) as well as its approximate counterpart deduced from the simulated 3D-IR spectrum both calculated along the same lines in  $(t_2, t_4)$ -space as the experiment and the same windowing function (eq 4) as the experiment (Figure 3b). Motional narrowing strongly suppresses the oscillatory inertial spike of  $c_3(t_2, t_4)$  at very early population times ( $t_2, t_4 < 200$  fs), but  $c_3(t_2, t_4)$  exhibits the same slowly relaxing tail afterward. The approximate  $c_3$  does not agree with every detail of the experiment, notably the initial value of  $c_3$  and the change in slope due to the many approximations involved. It does, however, reproduce the essential finding that it depends only on  $t_2 + t_4$ , and hence the extracted  $c_3$  gives evidence of the underlying heterogeneous dynamics (Figure 3b).

**Physical Picture.** The three-point correlation function directly suggests the existence of at least two discrete subensembles which strongly overlap in OD-stretch frequency but are separated along a “hidden coordinate” not directly accessed by the OD-stretching frequency (Figure 4a). The experimental  $c_3$  peaks at about 500 fs and then quickly decays to zero, so we conclude that these discrete subensembles have a typical lifetime of about half a picosecond. The  $c_3$ , however, provides neither a physical picture as of what the “hidden coordinate” might be nor the nature of the subensembles. Complex network analysis of an MD trajectory,<sup>56</sup> provides just such information. The output of the network analysis can be considered a model distilled from an MD simulation which includes all of the inherent complexity of the many degrees of freedom present in bulk water.

In our implementation of the complex network analysis,<sup>56</sup> we first run an MD simulation (Materials and Methods). We then assign to each water in the simulation a microstate based on the hydrogen bond connectivity extending to the second solvation shell. These microstates are the nodes of a transition network. When the hydrogen bonding pattern around a given water

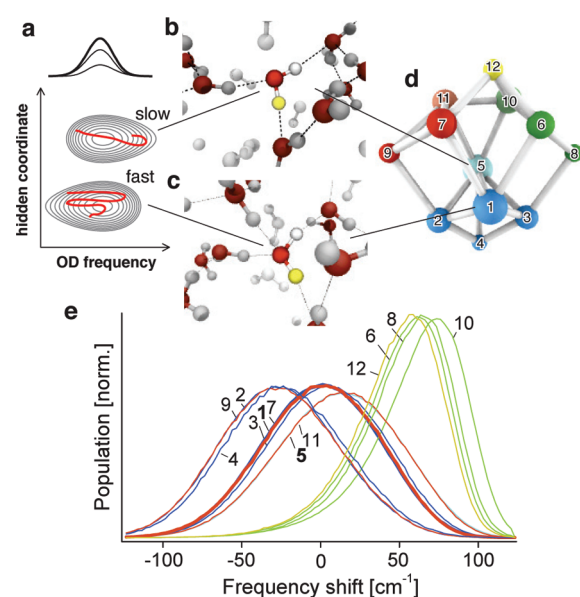


**Figure 4.** (a) The  $c_3$  extracted from the 3D-IR experiment is consistent with a model of at least two subensembles which have different rates of OD-stretch frequency fluctuations, which are each skewed to opposite directions and which mix on half a picosecond time scale. (b–c) An illustration of how different local environments could give rise to different structural relaxation rates. The OD is highlighted in yellow; the hydrogen bond network around the OD is shown up to two solvation shells, and other nearby waters (within  $\sim 5$  Å) are shown in white. (d) The hydrogen bond structures in b and c are representative of 2 of 12 free-energy basins identified by the complex network analysis.<sup>56</sup> (e) The 12 clusters have different characteristic frequencies for the OD stretch.

molecule changes, the resulting microstate also changes. These rearrangements are represented by links between nodes. The transition network is a representation of the observed configuration space and its dynamics. It is a high resolution mapping of the underlying free-energy landscape without projecting the system on a predefined reaction coordinate.

The nodes of this network are then clustered by their kinetic connectivity; that is, microstates which interconvert quickly are grouped together. These groups represent free-energy basins. We identified 12 such clusters which are separated by marginal barriers (see Figure 4d).<sup>56</sup> Note that some of these clusters are identical with respect to their immediate hydrogen bond partners but differ with respect to the hydrogen bond pattern in the second solvation shell. By varying the temperature in the MD simulation, we could furthermore determine whether each cluster is stabilized entropically or enthalpically.<sup>56</sup> These results are independent of water model used (SPC, SPC/E, TIP4P, TIPSP) and exact hydrogen-bond definition.<sup>56</sup>

Here, we propose that the heterogeneous dynamics we observe experimentally is related to exactly this partitioning of the water free energy surface into basins. First, the clusters revealed by the network analysis have different but highly overlapping distributions in OD stretching frequency (Figure 4e). Indeed, the characteristic lifetimes of these clusters is 200–400 fs,<sup>56</sup> in good agreement with our experiment.

Figure 4b,c illustrates the essential idea why water molecules in different clusters may be dynamically different, even though they cannot be unambiguously distinguished through their OD stretching frequency. Consider the two most populated clusters, labeled 1 and 5 (Figure 4d) that were identified by the complex network

analysis (however, one should keep in mind that many more than two such states are present at ambient conditions).<sup>36</sup> In the one case (Figure 4b), the OD chromophore (highlighted in yellow) and the OH are both engaged in hydrogen bonds, but the oxygen accepts only one hydrogen bond. In the other case (Figure 4c), the hydrogen is fully tetrahedral. The mean value of the OD frequency distributions in these two configurations are different only by  $\sim 15\text{ cm}^{-1}$  (Figure 4e). The different subensembles of water must be correlated with the OD-stretch frequency to some degree because of the sign change of  $c_3$  must shift the total OD-stretch frequency distribution's skewness in opposite directions (Figure 4a). This observation is consistent with the 2D-IR measurements of Steinell et al.<sup>21</sup> If different OD-stretch frequency regions did not have different rates of frequency fluctuations, then the  $c_3$  would always keep the same sign. But at no point are these subensembles clearly resolved along the OD-stretch frequency axis—there is never even a partially resolved bimodal distribution. Rather than resolve the subensembles based on their distinct frequencies, we detect them because of their different structural relaxation dynamics. 3D-IR spectroscopy can provide a new dimension because the additional population time acts as a selectivity filter not only based on distinguishable frequencies but also based on distinguishable structural relaxation dynamics.

Not all of the types of motions which lead to structural relaxation need be heterogeneous. The very fastest motions in water are librational in nature. The spike and oscillations in the exact  $c_3$  (Figure 3a), which are not a function of only  $t_2 + t_4$ , most likely represent the coupling of OH librational frequency to intermolecular O–O motions. The effect of these motions on the 3D-IR spectra, however, are suppressed by motional narrowing (Figure 3b). The motions we concentrate on here, on a 200–300 fs time scale (corresponding to 100–150  $\text{cm}^{-1}$ ) have been associated with local motions of the first solvation shell around a water molecule by the temperature dependence of THz spectra<sup>59,60</sup> as well as ab initio MD simulations.<sup>61</sup> This is consistent with our basic picture that the motions involve primarily reorganization within one hydrogen bonding motif (the clusters in the network analysis). Our results show that 3D-IR can at least partially decompose this highly overlapped spectral region and detect motions which are due to different hydrogen bonding motifs. Of course, we expect all motions in water slower than the typical interconversion time of the hydrogen bonding motifs (i.e., when, in eq 2  $T$  is greater than the average correlation time) to be homogeneous.

## CONCLUSIONS

The three-point correlation function is a function of two time-coordinates  $t_2$  and  $t_4$  and so is able to correlate various structural relaxation processes. This very fact constitutes the essential information gain of 3D-IR spectroscopy over 2D-IR spectroscopy. Higher-order correlation functions encode detailed and rich information about the dynamics of hydrogen bond rearrangements in liquid water, but they do so in a very subtle way. We therefore reiterate the line of reasoning of this paper:

- We find experimentally that the three-point correlation function changes sign and depends only on the sum of population times,  $t_2 + t_4$ . Two uncorrelated exponential relaxation processes have this property, as illustrated by the extremely simplified models in Figure 1d–e. We conclude that the isotope substituted liquid water is dynamically heterogeneous on a half picosecond time scale.

- Simulated 3D-IR spectra based on MD simulations of SPC water connected to line shape theory<sup>38,41</sup> qualitatively show the same result (Figure 3).
- Complex network analysis shows that the free energy surface of water is partitioned into basins characterized by the hydrogen bonding pattern extending into at least the second solvation shell. Marginal barriers stabilize these structures on a 200–400 fs time scale. We attribute the dynamical heterogeneity deduced from the three-point correlation function to this ruggedness of the water free energy surface.
- Given these results, we can now rationalize how different hydrogen-bond environments can affect the dynamics of the OD spectral diffusion (Figure 4b,c). Fastest are local librational motions on a  $\sim 50$  fs time scale; then relaxation within a free energy basin occurs, which we observe on half a picosecond time scale. Finally, the overall rearrangement of the hydrogen bond network on the 1–1.5 ps time scale consists of moving between free energy basins.

There is a long-standing and ongoing controversy about water inhomogeneity. For example, recent X-ray scattering (SAXS) experiments have been interpreted either as discrete structural heterogeneity<sup>4</sup> or just density fluctuations.<sup>7</sup> Our work may help resolve that disagreement. Clark et al.<sup>7</sup> argue that the SAXS data are consistent with the number density fluctuations expected from the isothermal compressibility. This need not be inconsistent with the picture we are proposing. Isothermal compressibility is one of the many anomalous thermodynamic properties of water. Debenedetti,<sup>62</sup> for example, connects each of these anomalies in liquid water to water's polymorphism (the amorphous solid water phases) and from there to the hypothesized liquid–liquid critical point. So if the interpretation of Clark et al.<sup>7</sup> is built on the compressibility, which includes the competition of structural motifs of low density and high density water, then perhaps density fluctuations need not rule out structural and dynamical heterogeneity of water. Clark et al.<sup>7</sup> continue and argue that the density distributions as a function of length scale are unimodal and ergo water is homogeneous. The network analysis in Rao et al.<sup>56</sup> has a completely different approach which separates these distributions in a natural way based on the calculated dynamics. The different structural motifs consistent with low density water and high density water naturally appear even though typical structural characterizations (radial distribution functions, for example, and by extension the density) simply cannot distinguish them. Structural heterogeneity can occur even though many one-dimensional observables, for example, density or vibrational line shape, do not directly provide bimodal distributions.

The distinction between fluctuations and heterogeneity must depend on the relevant time- and length scales. 3D-IR spectroscopy is able to observe different relaxation rates within different free energy basins and to estimate a half picosecond time scale for the interconversion of these subensembles, which reflects free energy barriers of the order of  $k_B T$ .<sup>56</sup> The fast interconversion time is probably also related to relatively small length scales (the size of which, however cannot be deduced from 3D-IR spectroscopy). In any case, 3D-IR spectroscopy constitutes an important new link between the static, structural characterization of water from scattering techniques and the dynamical characterization of the fast motions of water from ultrafast spectroscopy.

MD simulations have reproduced the correlation functions extracted from 2D-IR spectroscopy of isotope-diluted water with



considerable success and reveal a very mild dependence on the underlying force field.<sup>58</sup> The quality of agreement to 3D-IR spectroscopy is not as good and suggests that 3D-IR may prove a more critical test of the force fields as well as methods of simulating spectra. We hope that this work stimulates further theoretical effort.

## APPENDIX

**Data Analysis and Discussion.** Two-point correlation functions,  $c_2$ , can be extracted from 2D-IR spectra and simulations by many different quantitative measures, including ellipticity, dynamical linewidth, and nodal slope.<sup>63</sup> Similar geometrical measures of the 3D lineshape are related to  $c_2$  and *not* related to  $c_3$ . Recently, Jansen et al.<sup>64</sup> have proposed using the curvature of one of these metrics present in a 2D spectrum to access one part of the three-point correlation function, but these methods have not been extended to 3D.

Previous work<sup>41,39</sup> has shown that, in the limit of inhomogeneous broadening (i.e., that the effects of motional narrowing can be ignored), the ground state bleach and stimulated emission in an absorptive 3D-IR spectrum,  $R_1^{(S)}(\delta\omega_1, t_2, \delta\omega_3, t_4, \delta\omega_5)$  (Figure 2c, pathway 1), can be directly related to the joint probability density,  $\rho(\delta\omega_5|t_2 + t_4, \delta\omega_3|t_2, \delta\omega_1|0)$ , which is the probability of finding a water with frequency  $\delta\omega_5$  at time  $t_2 + t_4$  given that it was at frequency  $\delta\omega_3$  at time  $t_2$  given that it was at frequency  $\delta\omega_1$  at time 0, and where  $\delta\omega = \omega - \langle\omega\rangle$ . The three-point correlation function  $c_3$  can then be calculated directly via an integral over the 3D frequency space, eq 4. Water dynamics are clearly in an intermediate regime where motional narrowing and inhomogeneous broadening compete. Nevertheless, just like in 2D-IR spectroscopy, the three-point correlation function approximated in this way resembles the exact  $c_3$  for large enough delay times ( $t_2, t_4 \gtrsim 200$  fs).<sup>41</sup>

The integral in eq 4 is sensitive to the edges of the frequency distribution because it is weighted by the frequency cubed,  $\delta\omega^3$ . As a result, noise at the edges of the experimental spectra where there is no signal can dominate the extracted  $c_3$ . To control this error, the integrand in eq 4 is weighted by a windowing function, namely, a 150  $\text{cm}^{-1}$  broad Gaussian (full-width at half-maximum). This effectively concentrates the analysis on the dynamics at the center of the absorption band. An extension of the methods proposed by Jansen et al.<sup>64</sup> may in the future provide an approach which eliminates the need for this windowing procedure. In the comparison between the simulation and the experiment, all data have been treated with the same windowing function.

The other pathways (Figure 2c, pathways 2–5) should *not* be included in calculating eq 4 and need to be eliminated. The negative features of pathway 2 (Figure 2b, blue) are eliminated by filtering out all points in the spectrum which are negative. The band itself is removed, but it still perturbs the ground state bleach. Response functions from MD simulations have shown that this remaining effect is primarily to reduce the absolute magnitude of  $c_3$ , but there is also a  $\sim 20\%$  difference in  $c_3$  along the diagonal versus along an  $t_2$  axis.

On the other hand, the presence of a band corresponding to pathway 5, when overlapping with band 1, could qualitatively change the appearance of  $c_3$ , even causing it to change sign if it were present at the intensity given by the harmonic estimate. However, as discussed below, this band is strongly suppressed in the data. At or below the 0.15 times the harmonic estimate for the intensity, this band causes only a  $\sim 10\%$  change in the amplitude

of the extracted  $c_3$  based again on response functions calculated through MD simulations.<sup>38</sup>

The fastest motions in the liquid, librational motions are not observed in this measurement of  $c_3$  because of motional narrowing. The essential time resolution of the experiment is not determined solely by the pulse duration. It takes a finite amount of time,  $\Delta t$ , to record a frequency splitting of  $\Delta\omega = 2\pi/\Delta t$  in each coherence time. Microscopic dynamics which occur during this time cannot be clearly differentiated. The minimum effective time resolution then given by the dephasing times in  $t_1, t_3$ , and  $t_5$  set the minimum time interval which can be measured  $\sim 200$  fs. Motions faster than this time scale, such as librational motions, are in the motional narrowing limit and cannot be extracted from the analysis of 3D-IR spectra described above.

**Presence of Excited State Absorptions (Pathway 5).** The intensity ratios of the vibrational bands in a 3D experiment were previously described.<sup>39</sup> Briefly, the intensity can be estimated by counting the number of Feynman diagrams corresponding to each vibrational band and scaling by the transition dipole moment (which increases with vibrational quantum number). Calculations based on the fifth-order response function from previous MD simulations<sup>39</sup> suggest that, at an amplitude of  $\sim 0.15$  the harmonic estimate, these vibrational bands corresponding to peak 5 should be seen as a protrusion in the lowest contour levels in the projections of the 3D spectrum, which are not observed. We attribute this to differences in dynamics (i.e., the peak is broader) and transition dipole (i.e., the peak is weaker). The excited vibrational states of water are known to be extremely anharmonic,<sup>65</sup> and, as such, it is perhaps not surprising that simple estimates based on a weakly perturbed harmonic oscillator model are inaccurate.

**Presence of Cascaded Third-Order Signals.** Cascading third-order signals are a possible contaminant in fifth-order spectroscopy, and it is important to carefully determine their contribution to higher order spectroscopic signals. The strongest experimental verification that the measured signal comes from direct fifth-order signals rather than cascaded third-order signal is the variation of the signal amplitude with concentration. A direct fifth-order signal scales linearly with the concentration because it originates from independent non-interacting chromophores. A cascaded signal, however, scales quadratically with the concentration because one chromophore emits a field which is absorbed by another. Figure 5 shows a linear dependence of signal amplitude on concentration, demonstrating that the fifth-order signals dominate the cascades at the experimental conditions used here.

Previous 3D-IR experiments agree with this conclusion. Zanni et al.<sup>57</sup> demonstrated that, for azide in a glassy matrix, cascades did not contribute to a two-quantum 3D-IR pulse sequence ( $< 5\%$ ), and in our lab, we showed the same for absorptive 3D-IR for the asymmetric stretch of  $\text{CO}_2/\text{H}_2\text{O}$ .<sup>39</sup>

The ratio of a cascaded third-order signal to direct fifth-order signal can be estimated as,<sup>44,57</sup>

$$\frac{E^{(\text{cas})}}{E^{(5)}} = -\frac{\omega L \hat{N} \mu^2}{2nc\epsilon_0 \hbar} \frac{d_5}{d_3^2} \frac{g_{\text{cas}}}{g_5} \times \frac{[\{E_1, E_2, E_3\} \otimes R^{(3)}] \otimes [\{E_4, E_5\} \otimes R^{(3)}]}{\{E_1, E_2, E_3, E_4, E_5\} \otimes R^{(5)}} \quad (5)$$

Here, the  $d_n$  are the direction cosines, that is,  $d_3 = 5$  and  $d_5 = 7$ . The terms  $g_{\text{cas}}$  and  $g_5$  represent the number of Feynman diagrams

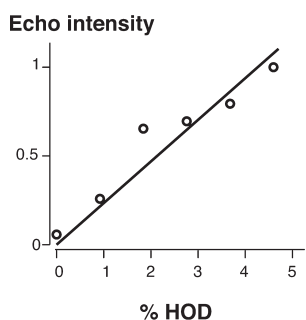


**Figure 5.** The 3D-IR signal intensity increases linearly with the HOD concentration.

which contribute for cascaded and direct processes, and  $g_{\text{cas}}/g_5 = 2$  because of the combination of sequential and parallel pathways. Here the notation  $\{E_1, \dots, E_n\} \otimes R^{(n)}$  represents the  $n$ -time convolution of the pump pulses with the material response. The response functions  $R^{(3)}$  and  $R^{(5)}$  are, per se, unitless and initially magnitude 1. Phase-matching has only a small effect in the IR because the experiment is a degenerate wave-mixing experiment and because the sample path lengths are short. For this reason, the phase matching term  $f(\Delta k l/2) \sim 1^{67}$  for both cascades and the direct fifth-order signal is negligible.

The convolutions in the numerator and denominator of eq 5 will each depend on the magnitude and duration of the five pump electric fields, so these contributions cancel. The remaining convolution of  $R^{(3)} \otimes R^{(3)}$  is roughly proportional to the time scale of the decay of the macroscopic induced polarization, or the free-induction decay,

$$R^{(3)} \otimes R^{(3)} = \Delta t_{\text{tot}} \quad (6)$$

which depends on the total width of the transition (including the inhomogeneous width)  $\Delta t_{\text{tot}} = \pi \Delta \nu_{\text{tot}}$  or

$$R^{(3)} \otimes R^{(3)} = \frac{1}{\pi \Delta \nu_{\text{tot}}} \quad (7)$$

The integrated molar absorption coefficient,  $A$ , is

$$\mathcal{A} = \int d\nu \varepsilon(\nu) \quad (8a)$$

$$= A_{\text{peak}} \Delta \nu_{\text{hom}} \frac{\pi N_A}{2 \mathcal{N} l} \quad (8b)$$

$$= \frac{\pi \bar{\nu}}{3 \ln(10) n c \varepsilon_0} \left( \frac{N_A \mu^2}{\hbar} \right) \quad (8c)$$

where  $\Delta \nu_{\text{hom}}$  is the homogeneous linewidth of the transition, and  $N_A$  is Avogadro's number. The step from eq 8a to eq 8b assumes that only the molecules within the homogeneous linewidth share a common transition dipole, and the integration of a Lorentzian line gives  $\pi/2$ . Using eqs 7, 8b, and 8c, we can rearrange eq 5 to the following:

$$\frac{E^{(\text{cas})}}{E^{(5)}} = - \frac{3 \ln(10)}{2} \frac{\Delta \nu_{\text{hom}}}{\Delta \nu_{\text{tot}}} \frac{d_5}{d_3^2} \frac{g_{\text{cas}}}{g_5} A_{\text{peak}} \quad (9)$$

Equation 9 shows that the cascading amplitude will be small for optically thin samples. Essentially, the cascading process can be seen as an unintended absorption occurring halfway through the

pulse sequence. As long as the sample is optically thin, this reabsorption effect will remain a minor contribution.

The current experiment is done at a total optical density of  $\sim 0.3$ , (the sum of the OD-stretching band,  $A_{\text{peak}} = 0.2$  and the broad  $\text{H}_2\text{O}$  background  $A_{\text{bg}} = 0.1$ ). This is at the border of what is optically thin. The effects of absorption of the pump light through the sample thickness and reabsorption of the signals can also be calculated. The numerical result is that the absorption of pump light tends to limit the relative intensity of the cascaded to direct signals. Essentially, the relative magnitude of the cascade cannot increase once the third-order signal has reached its maximum (OD  $\sim 0.5$ ). At this point all fields are dominated by (linear) reabsorption. For our experimental conditions, numerical modeling of the sample reabsorption decreases the ratio of cascade to direct signal by another factor of 0.65. Combining these factors, the cascading will then contribute to  $\sim 10\%$  of the total signal.

## ■ ASSOCIATED CONTENT

**Supporting Information.** Movies display the 3D shape of the spectra taken at population times  $(t_2, t_4) = (100, 100)$  fs and  $(t_2, t_4) = (300, 300)$  fs (qt format). This material is available free of charge via the Internet at <http://pubs.acs.org>.

## ■ AUTHOR INFORMATION

### Corresponding Author

\*E-mail: [phamm@pci.uzh.ch](mailto:phamm@pci.uzh.ch).

## ■ ACKNOWLEDGMENT

We thank A. Nilsson and D. Nordlund for an initial cartoon depicting of heterogeneous dynamics (Figure 4b–c). The work was supported by the Swiss National Science Foundation (SNF) through the NCCR MUST. S.G.R. was partially supported by the National Science Foundation (USA) under Grant OISE-0601907. Calculations were performed on the Schrödinger computer cluster of the University of Zurich.

## ■ REFERENCES

- (1) Röntgen, W. C. *Ann. Phys. Chem.* **1892**, 281, 91–97.
- (2) Giovambattista, N.; Buldyrev, S.; Starr, F.; Stanley, H. *Phys. Rev. Lett.* **2003**, 90, 85506.
- (3) Chandler, D.; Garrahan, J. P. *Annu. Rev. Phys. Chem.* **2010**, 61, 191–217.
- (4) Huang, C.; *Proc. Natl. Acad. Sci. U.S.A.* **2009**, 106, 15214–15218.
- (5) Soper, A. K.; Teixeira, J.; Head-Gordon, T. *Proc. Natl. Acad. Sci. U.S.A.* **2010**, 107, E44.
- (6) Huang, C.; *Proc. Natl. Acad. Sci. U.S.A.* **2010**, 107, E45.
- (7) Clark, G. N. I.; Hura, G. L.; Teixeira, J.; Soper, A. K.; Head-Gordon, T. *Proc. Natl. Acad. Sci. U.S.A.* **2010**, 107, 14003–14007.
- (8) Woutersen, S.; Emmerichs, U.; Bakker, H. J. *Science* **1997**, 278, 658.
- (9) Laenen, R.; Rauscher, C.; Laubereau, A. *Phys. Rev. Lett.* **1998**, 80, 2622–2625.
- (10) Gale, G. M.; Gallot, G.; Hache, F.; Lascoux, N.; Bratos, S.; Leicknam, J. C. *Phys. Rev. Lett.* **1999**, 82, 1068–1071.
- (11) Rey, R.; Moller, K. B.; Hynes, J. T. *J. Phys. Chem. A* **2002**, 106, 11993–11996.
- (12) Fecko, C. J.; Eaves, J. D.; Loparo, J. J.; Tokmakoff, A.; Geissler, P. L. *Science* **2003**, 301, 1698–1702.
- (13) Yeremenko, S.; Pschenichnikov, M. S.; Wiersma, D. A. *Chem. Phys. Lett.* **2003**, 369, 107–113.



- (14) Moller, K. B.; Rey, R.; Hynes, J. T. *J. Phys. Chem. A* **2004**, *108*, 1275–1289.
- (15) Wang, Z. H.; Pakoulev, A.; Pang, Y.; Dlott, D. D. *J. Phys. Chem. A* **2004**, *108*, 9054–9063.
- (16) Asbury, J. B.; Steinel, T.; Stromberg, C.; Corcelli, S. A.; Lawrence, C. P.; Skinner, J. L.; Fayer, M. D. *J. Phys. Chem. A* **2004**, *108*, 1107–1119.
- (17) Cowan, M. L.; Bruner, B. D.; Huse, N.; Dwyer, J. R.; Chugh, B.; Nibbering, E. T. J.; Elsaesser, T.; Miller, R. J. D. *Nature* **2005**, *434*, 199–202.
- (18) Auer, B.; Schmidt, J. R.; Skinner, J. L. *Proc. Natl. Acad. Sci. U.S.A.* **2007**, *104*, 14215–14220.
- (19) Steinel, T.; Asbury, J. B.; Zheng, J. R.; Fayer, M. D. *J. Phys. Chem. A* **2004**, *108*, 10957–10964.
- (20) Geissler, P. L. *J. Am. Chem. Soc.* **2005**, *127*, 14930–14935.
- (21) Steinel, T.; Asbury, J. B.; Corcelli, S. A.; Lawrence, C. P.; Skinner, J. L.; Fayer, M. D. *Chem. Phys. Lett.* **2004**, *386*, 295–300.
- (22) Brubach, J. B.; Mermet, A.; Filabozzi, A.; Gerschel, A.; Roy, P. *J. Chem. Phys.* **2005**, *122*, 184509.
- (23) Smith, J. D.; Cappa, C. D.; Wilson, K. R.; Cohen, R. C.; Geissler, P. L.; Saykally, R. J. *Proc. Natl. Acad. Sci. U.S.A.* **2005**, *102*, 14171–14174.
- (24) Eaves, J. D.; Loparo, J. J.; Fecko, C. J.; Roberts, S. T.; Tokmakoff, A.; Geissler, P. L. *Proc. Natl. Acad. Sci. U.S.A.* **2005**, *102*, 13019–13022.
- (25) Kropman, M. F.; Bakker, H. J. *Science* **2001**, *291*, 2118–2120.
- (26) Park, S.; Fayer, M. D. *Proc. Natl. Acad. Sci. U.S.A.* **2007**, *104*, 16731–16738.
- (27) Moilanen, D. E.; Fenn, E. E.; Lin, Y.-S.; Skinner, J. L.; Bagchi, B.; Fayer, M. D. *Proc. Natl. Acad. Sci. U.S.A.* **2008**, *105*, 5295–5300.
- (28) Rezus, Y. L. A.; Bakker, H. J. *Phys. Rev. Lett.* **2007**, *99*, 148301.
- (29) Laage, D.; Stirnemann, G.; Hynes, J. T. *J. Phys. Chem. B* **2009**, *113*, 2428–2435.
- (30) Bakulin, A. A.; Liang, C.; Jansen, T. L.; Wiersma, D. A.; Bakker, H. J.; Pshenichnikov, M. S. *Acc. Chem. Res.* **2009**, *42*, 1229–1238.
- (31) Novak, A. In *Structure and bonding*; Dunitz, J. D., Hemmerich, P., Holm, R. H., Ibers, J. A., Jorgenson, C. K., Neilands, J. B., Reinen, D., Williams, R. J. P., Eds.; Springer-Verlag: New York, 1974.
- (32) Eaves, J. D.; Tokmakoff, A.; Geissler, P. L. *J. Phys. Chem. A* **2005**, *109*, 9424–9436.
- (33) Laage, D.; Hynes, J. T. *Science* **2006**, *311*, 832–835.
- (34) Paesani, F.; Xantheas, S. S.; Voth, G. A. *J. Phys. Chem. B* **2009**, *113*, 13118–13130.
- (35) van Veldhoven, E.; Khurmi, C.; Zhang, X.; Berg, M. A. *ChemPhysChem* **2007**, *8*, 1761–1765.
- (36) Bredenbeck, J.; Helbing, J.; Hamm, P. *Phys. Rev. Lett.* **2005**, *95*, 083201.
- (37) Garrett-Roe, S.; Hamm, P. *Acc. Chem. Res.* **2009**, *42*, 1412–1422.
- (38) Garrett-Roe, S.; Hamm, P. *J. Chem. Phys.* **2008**, *128*, 104507.
- (39) Garrett-Roe, S.; Hamm, P. *J. Chem. Phys.* **2009**, *130*, 164510.
- (40) Underwood, D. F.; Blank, D. A. *J. Phys. Chem. A* **2003**, *107*, 956–961.
- (41) Hamm, P. *J. Chem. Phys.* **2006**, *124*, 124506–124518.
- (42) Golonzka, O.; Demirdöven, N.; Khalil, M.; Tokmakoff, A. *J. Chem. Phys.* **2000**, *113*, 9893–9896.
- (43) Blank, D. A.; Kaufman, L. J.; Fleming, G. R. *J. Chem. Phys.* **2000**, *113*, 771–778.
- (44) Kubarych, K. J.; Milne, C. J.; Miller, R. J. D. *Int. Rev. Phys. Chem.* **2003**, *22*, 497–532.
- (45) Yagasaki, T.; Saito, S. *Acc. Chem. Res.* **2009**, *42*, 1250–1558.
- (46) Kim, K.; Saito, S. *J. Chem. Phys.* **2010**, *133*, 044511.
- (47) Schmidt-Rohr, K.; Spiess, H. W. *Phys. Rev. Lett.* **1991**, *66*, 3020–3023.
- (48) Demirdöven, N.; Khalil, M.; Golonzka, O.; Tokmakoff, A. *Opt. Lett.* **2002**, *27*, 433–435.
- (49) Fulmer, E. C.; Mukherjee, P.; Krummel, A. T.; Zanni, M. T. *J. Chem. Phys.* **2004**, *120*, 8067–8078.
- (50) Bloem, R.; Garrett-Roe, S.; Strzalka, H.; Hamm, P.; Donaldson, P. *Opt. Express* **2010**, *18*, 27067.
- (51) Bartholdi, E.; Ernst, R. R. *J. Magn. Reson.* **1973**, *11*, 9–19.
- (52) Backus, E.; Garrett-Roe, S.; Hamm, P. *Opt. Lett.* **2008**, *33*, 2665–2667.
- (53) Lindahl, E.; Hess, B.; van der Spoel, D. *J. Mol. Modell.* **2001**, *7*, 306–317.
- (54) Oxtoby, D. W.; Levesque, D.; Weis, J.-J. *J. Chem. Phys.* **1978**, *68*, 5528–5533.
- (55) Smith, J. D.; Saykally, R. J.; Geissler, P. L. *J. Am. Chem. Soc.* **2007**, *129*, 13847–13856.
- (56) Rao, F.; Garrett-Roe, S.; Hamm, P. *J. Phys. Chem. B* **2010**, *114*, 15429–15722.
- (57) Fulmer, E. C.; Ding, F.; Zanni, M. T. *J. Chem. Phys.* **2005**, *122*, 034302.
- (58) Schmidt, J. R.; Roberts, S. T.; Loparo, J. J.; Tokmakoff, A.; Fayer, M. D.; Skinner, J. L. *Chem. Phys.* **2007**, *341*, 143–157.
- (59) Ronne, C.; Thrane, L.; Astrand, P.; Wallqvist, A.; Mikkelsen, K.; Keiding, S. *J. Chem. Phys.* **1997**, *107*, 5319–5331.
- (60) Ronne, C.; Astrand, P.; Keiding, S. *Phys. Rev. Lett.* **1999**, *82*, 2888–2891.
- (61) Heyden, M.; Sun, J.; Funkner, S.; Mathias, G.; Forbert, H.; Havenith, M.; Marx, D. *Proc. Natl. Acad. Sci. U.S.A.* **2010**, *107*, 12068–12073.
- (62) Debenedetti, P. *J. Phys.: Condens. Matter* **2003**, *15*, R1669–R1726.
- (63) Roberts, S. T.; Loparo, J. J.; Tokmakoff, A. *J. Chem. Phys.* **2006**, *125*, 084502.
- (64) Roy, S.; Pshenichnikov, M. S.; la Cour Jansen, T. *J. Phys. Chem. B* **2011**, *115*, 5431–5440.
- (65) Bakker, H. J.; Nienhuys, H. K. *Science* **2002**, *297*, 587–590.
- (66) Mukamel, S. *Principles of Nonlinear Optical Spectroscopy*; Oxford University Press: New York, 1995.
- (67) Ref 66, p 98.